# Isomeric Structures of Isolated Ammonium Nitrate and Its Hydrogenated Species Identified Through PES Experiments and DFT Calculations

SCHOLARONE™
Manuscripts

# Isomeric Structures of Isolated Ammonium Nitrate and Its Hydrogenated Species Identified Through PES Experiments and DFT Calculations

Zhen Zeng, Elliot R. Bernstein*

*Department of Chemistry, NSF ERC for Extreme Ultraviolet Science and Technology, Colorado State University, Fort Collins, CO 80523, USA*

ABSTRACT

Anion photoelectron spectroscopic (PES) experiments in conjunction with density functional theory (DFT) calculations shed light on the electronic and geometric structures of gas phase, isolated ammonium nitrate related anionic species, as well as their hydrogenated species with up to five added hydrogens. These species are directly generated by laser ablation and cooled in a supersonic expansion. Their vertical detachment energies (VDE: $E_{neutral} - E_{anion}$, both at the anionic geometry) are experimentally determined and the corresponding anionic structures are characterized and assigned through calculations. Based on the experimentally evaluated calculation algorithm, the corresponding neutral structures are also determined. The parent anionic species exists as $(NH_2OH \bullet HONO)^-$ in the gas phase with the extra electron valence bound. Crystal structure anion $NH_4NO_3^-$ is not present in our experiments, as within this structure the extra electron is dipole bound (electron affinity ~ 0 eV). The isomerization must therefore occur for ammonium nitrate upon capturing an extra electron or during the laser ablation process itself. The ammonium nitrate anion is apparently a very reactive species. The calculated global minimum for the isolated parent neutral species has an $HNO_3 \bullet NH_3$ structure, different from the crystal structure in the bulk phase. The hydrogenated cluster anions can evolve from the parent $(NH_2OH \bullet HONO)^-$ species and exhibit moieties, which bind together as a single unit through interactions between noncovalently bonded species and are stable on the experimental timescale. The hydrogenation process forms stable moieties in the cluster anions, including water ($H_2O$), nitroxyl (HNO), ammonia ($NH_3$), or (HNOH). The calculated global minimum structures for hydrogenated cluster neutrals ($NH_4NO_3$ + nH, n = 1,…,5) contain ammonia and water, along with stable moieties (HONO, NO, and HNO). These stable moieties, along with intermediate species $NO_2H_2$ and

$ONH_2$, offer new insights into the behavior of ammonium nitrate energetic materials.

## I. INTRODUCTION

Ammonium nitrate ($NH_4NO_3$) is universally employed as an important agricultural fertilizer, and readily forms explosive mixtures along with various fuels and primary explosives. Ammonium nitrate has also been identified as an atmospheric aerosol component associated with air pollutants.[1-4] Condensed phase ammonium nitrate is likely to vaporize by decomposing into $NH_3$ and $HNO_3$. These components are additionally utilized as ingredients in automobile air bags.

Given the ubiquitous application of ammonium nitrate throughout numerous industries, industrial, regulatory and academic researchers have long sought to quantify the safety and security hazards associated with the production, transportation, application, management, storage, and misuse of the material, and tried to learn lessons from ammonium nitrate disasters.[5-7] Due to the complex nature of the decomposition reactions, which follow an initiation event, however, significant limitations arise when researchers seek to understand and predict the behavior of the material. Research clarifying the core mechanisms that advance ammonium nitrate from a stable salt through energy release to decomposition products is essential to enable the safest possible application of the material.

Ammonium nitrate (see Figure 1) has been the object of numerous thermal decomposition studies associated with its usage as an oxidizer or energetic component of both propellants and explosives. By using simultaneous torsion-effusion/mass loss methods to analyze the vapor over solid phase $NH_4NO_3$, mass signals for $NH_4NO_3(g)$, $NH_3(g)$, and $HNO_3(g)$, are detected. These observations demonstrate that the vapor above solid ammonium nitrate includes the molecule $NH_4NO_3$, as well as decomposition products $NH_3$ and $HNO_3$.[8, 9]

Many studies have been performed to investigate the thermal decomposition products and/or their appearance kinetics.[10-16] Based on a rapid-scan FTlR/thermal profiling technique at various pressures and heating rates, the decomposition gas products can be of an endothermic and/or exothermic degradation nature, and include $HNO_3$, $NH_3$, $NO_2$, $NO$, $H_2O$ and/or $N_2O$.[17] A thermogravimetry experiment was conducted to study the kinetics of decomposition and vaporization for both solid and liquid ammonium nitrate:[18] both phases evidence similar kinetics of thermal gasification, ($NH_4NO_3(s) \leftrightarrow NH_3(g) + HNO_3(g)$). Furthermore, secondary reactions of ammonia and nitric acid can generate $N_2O$ and $H_2O$ through an exothermic channel.[10, 11, 18, 19] A recent theoretical study designed to characterize the gas phase decomposition mechanisms of ammonium nitrate, identifies five

reaction channels, yielding the experimentally characterized compounds $N_2$, $H_2O$, $O_2$, OH, HNO, $NO_3$.[20] Decomposition mechanisms for generation of gaseous products of $NH_4NO_3$ must include initial reaction mechanisms associated with different potential initiation/triggering processes (e.g., shock, impact, thermal excitation, and excited electronic neutral and ionic (+/-) states). In general, initiation processes can be related to triboluminescence (TL) phenomenon,[21] which generates emission of light from materials by the application of mechanical stress, and involves creation of charged and neutral atoms, molecules, fragments, radicals, as well as electrons and protons. The energy associated with such species can readily induce breaking of intra- and inter-molecular bonds.  Thus, neutral electronic excited states and ions are also important initiation pathways for the energetic molecule. To the best of our knowledge, anions, cations, and excited neutral states of ammonium nitrate have not as yet been investigated with regard to the energy initiation/release mechanisms for these energy storage systems.

Laser ablation/spectroscopic studies of ammonium nitrate have been executed in order to study decomposition product populations. By using rapid temperature jump laser ablation (~35-65 mJ for 1054 nm, 20-30 mJ for 532 nm, and 6-12 mJ for 266 nm) coupled with argon matrix trapping and FTIR absorption spectroscopy, different laser energies and wavelengths evidence different product populations, for $NH_3$, $HNO_3$, NO, $NO_2$, $N_2O$, and aggregates.[22] Laser induced breakdown spectroscopy (LIBS), employing high energy nanosecond pulsed lasers to generate plasmas, is widely used to analyze for ammonium nitrate.[23, 24] Numerous transitions of neutral atomic nitrogen are characterized from the emission spectrum of ammonium nitrate plasma generated in the LIBS study: spatial behavior of the plasma electron temperature and electron number density can also be determined.[25] The structural characteristics of isolated (-/0/+) ammonium nitrate remain to be understood at low energy laser irradiation, different from the previous laser ablation/spectroscopic studies with high laser ablation energy. Under these more gentle conditions initial dissociation mechanisms can be revealed, as well, which can be related to the low impulse or slow thermal initiation dissociation mechanism.

In the present study, we report anion photoelectron spectroscopy (PES) studies with density functional theory analysis for parent anionic species of ammonium nitrate and their hydrogenated cluster anions with up to 5 hydrogens. These approaches enable characterization of their electronic and geometric structures. The observed anionic, isolated gas phase structures are assigned by PES and DFT

studies. The corresponding neutral species are also provided based on the evaluated (through VDEs) DFT algorithm. The newly discovered hydrogenated clusters and their parent anionic species, as recorded in this present study, shed light on reactive intermediates and fragmentation products for the reaction/dissociation mechanisms of gas and solid phase ammonium nitrate. These findings generate a clearer and more complete description of ammonium nitrate initiated energetics.

## II. EXPERIMENTAL PROCEDURES

The experimental apparatus consists of three parts: a pulsed supersonic nozzle with an attached matrix assisted laser desorption ionization (MALDI) source, a reflectron time of flight mass spectrometer (RTOFMS), and a magnetic bottle photoelectron TOF spectrometer (MBTOFPES). Details of this system (RTOFMS/MBTOFPES) can be found in our previous publications.[26, 27] The nozzle employed for the sample beam generation is constructed from a Jordan Co. pulsed valve with a home made laser desorption attachment. Sample drums for the matrix assisted laser desorption and ionization (MALDI) process are prepared by wrapping sample desorption substrate Zn on a clean Al drum.[28] A mixed solution of ammonium nitrate and matrix (R6G or DCM) dye with mole ratio ~ 1:2 in a solvent (typically, acetonitrile and water) is uniformly sprayed on the drum/substrate surface using an air atomizing spray nozzle (Spraying System Co.) with siphon pressure of 10 psig. During the spraying process, the sample drum is rotated under heat of a halogen lamp (< 70 °C) in a fume hood to ensure deposition of ammonium nitrate and matrix on the drum surface is homogeneous and dry. The well coated and dried sample drum is then placed in the laser ablation head/nozzle assembly and put into the vacuum chamber. Second harmonic (532 nm) light pulses from a Nd:YAG laser are used to ablate the sample drum, which rotates and translates simultaneously to maintain a fresh sample area for each laser ablation pulse. Whole ammonium nitrate molecules are desorbed from the drum, interact with other species (including electrons) in the ablated material plume, are entrained in the supersonic flow of helium carrier gas with a 50 psi backing pressure through a $2 \times 60$ mm channel in the ablation head, and expanded into the sample chamber. For directly ablating a pure ammonium nitrate sample with no dye molecules present, the dried pure ammonium nitrate sample drum is made by spraying pure ammonium nitrate water solution and evaporating solvents. With a closed pulsed valve, the RTOFMS chamber pressure is ~ $6 \times 10^{-8}$ Torr. Generated molecular

anions are pulsed into the RTOFMS and are mass analyzed using the RTOFMS. For PES experiments, specific anions are first mass selected and decelerated before interacting with a 355 nm (3.496 eV), or 266 nm (4.661 eV) laser beam from another Nd:YAG laser in the photodetachment region. Photodetached electrons are collected and energy analyzed by the MBTOFPES at nearly 100% efficiency. The photodetachment laser is operated at a 10 Hz repetition rate, while the ablation laser is synchronously triggered at 5 Hz. Data are collected at 5 Hz employing a background subtraction with alternation of the ablation laser on/off if the detachment laser wave length is equal to or less than 266 nm. Every photoelectron spectrum is calibrated by the known spectra of Cu⁻ at the employed detachment photon energy. The photoelectron energy resolution is ~ 4% (40 meV for 1 eV kinetic energy electrons), as anticipated for a 1 m PES flight tube.

## III COMPUTATIONAL METHODS

In the present work, all calculations are executed using density function theory (DFT) employing $\omega$B97XD[29] and M062X[30, 31] functionals with Dunning's correlation consistent aug-cc-pvtz basis set for all atoms, as implemented in the Gaussian 09 program.[32] The $\omega$B97XD functional is a long-range-corrected hybrid functional with additional dispersion corrections, which has been evaluated for accurate prediction of properties of non covalently bonded interacting system.[33, 34] No symmetry restrictions are applied for the calculations. Optimization of the low lying isomers for each anion and neutral are performed with harmonic vibrational frequencies calculated to confirm that the obtained structures are the true local minima. Theoretical VDEs for each anionic species are calculated as the energy difference between the ground state of the anion and its corresponding neutral at the same structure as the anion. For further electronic structure based understanding of the observed ammonium nitrate related species behavior, a Natural Bond Orbital (NBO, also from Gaussian 09 program) analysis is performed based on the $\omega$B97XD functional and the aug-cc-pvtz basis set. The calculation for binding energy of molecular clusters are also conducted at the $\omega$B97XD/aug-cc-pvtz level of theory, for which the basis set superposition error (BSSE) can be ignored, see supplementary material Table S1. The geometries of hydrogenated cluster species are optimized by adding an H atom to the parent species and smaller size hydrogenated species at every possible position.

## IV. EXPERIMENTAL RESULTS

Through laser ablation directly on the ammonium nitrate solid sample surface, the parent anion and hydrogenated cluster anions with up to 5 hydrogens can be generated and are observed in the reflectron TOF mass spectrum (see Figure 2). The dissociation ions ($NO_3^-$, $NO_2^-$) and some carbon contained molecule/clusters impurities ($CN^-$, $C_4H_{0-2}$) are also obviously observed. The photoelectron spectra of parent anion and its hydrogenated cluster anions $(NH_4NO_3 + nH)^-$ (n = 0-5) recorded with 355 nm photons are presented in Figure 3. VDEs are measured from the maxima of the corresponding PES peaks. The VDEs of $(NH_4NO_3 + nH)^-$ (n = 0-5) anionic species are summarized in Table 1. The photoelectron spectrum of parent anionic species shows a single peak, centered at 2.18 eV. The photoelectron spectra of hydrogenated cluster anions $(NH_4NO_3 + nH)^-$ (n = 1-5) all display broad structureless PES features. These spectra suggest at least one of two possible situations: 1. overlapped vibrational and/or rotational transitions with large geometry changes between the anion and neutral; and/or 2. different isomers coexisting in the ablated, cooled sample. The photoelectron spectrum of $(NH_4NO_3 + H)^-$ displays peak centered at 1.72 eV, lower than that of parent anion. The photoelectron spectrum of $(NH_4NO_3 + 2H)^-$ exhibits a broad and flattop shaped feature, which can also be indicative of many different coexisting isomers, with VDEs centered from ~2.13 eV to ~2.63 eV. The PES features of $(NH_4NO_3 + nH)^-$ (n = 3-5) are centered at ~1.88, ~2.35, and ~1.91 eV, respectively. The experimental VDEs vary in a "Z" like pattern, which shows the experimental VDE decreases and increases alternatively. Using higher energy photons (266 nm), no higher electron binding energy PES features can be detected for $(NH_4NO_3 + nH)^-$ (n = 0-2), as can be seen from supplementary material Figure S20.

Through MALDI/ablation processes, only $(NH_4NO_3 + H)^-$ anionic species can be observed in the mass spectrum, as shown in Figure S21 of supplementary material. Its photoelectron spectrum shows a narrower peak also centered at ~1.72 eV, compared to the PES feature from laser ablating an $NH_4NO_3$ sample directly. The MALDI/ablation source, with an absorbing dye matrix, provides a gentler method for the generation of a target species than does direct ablation of the pure sample.

## V. THEORETICAL RESULTS

The low energy isomers of $(NH_4NO_3 + nH)^-$ (n = 0-5) are optimized via ωB97XD/aug-cc-pvtz and M062X/aug-cc-pvtz DFT approaches. From these two

density functionals, we can obtain consistent assignments of every specific species, as shown in Table 1, and nearly identical geometrical structures, as can be seen in Figures 4, 5, 7-10 and S14-S19. ωB97XD/aug-cc-pvtz results show calculated VDEs closer to experiments than does M062X/aug-cc-pvtz. Therefore, ωB97XD/aug-cc-pvtz level of theory is chosen for interpreting and exploring the theoretical results.

Theoretical results for the low lying isomers of $(NH_4NO_3 + nH)^-$ (n = 0-5) anions, as well as their corresponding neutrals, are summarized in Figures 4 to 10 and Table 1. Calculated and experimental VDEs are also compared in this table: a ± ~ 0.3 eV difference is considered to be reasonable agreement based on a calculational error of 0.2 eV for both anion and neutral species, and the observed broad spectral feature. With increasing number of H atoms (n = 4, 5), higher variances can be anticipated as more interactions between noncovalently bonded species are evolved. More isomers are presented in the supplementary material.

**a) parent species**

Four low lying isomers of parent anionic species are shown in Figure 4I. The lowest energy isomer (A) shows $NO_2$, OH, and $NH_3$ groups bound together. Its calculated VDE is 3.83 eV, significantly higher than the experiment features, and thus this isomer must not be present in the experimental sample. Isomer (B) has a relative energy of 0.69 eV, with a crystal-like structure for $NH_4NO_3$. It has a very low calculated VDE of 0.45 eV, not seen in the spectrum, and it too can be eliminated as a component of the experimental sample. Isomer C has a relative energy of 0.79 eV, displaying a structure with hydroxylamine ($NH_2OH$) and nitrous acid (HONO) moieties. (see Table S2 for the moiety names). The calculated VDE of isomer C is 2.07 eV, which is in excellent agreement with the experimental result (2.18 eV). Isomer D has nearly degenerate energy to that of isomer C, as well as similar structure, but with different OH bond orientation. Its theoretical VDE is 2.10 eV, also in good agreement with the experimental observation. Thus, the photoelectron spectrum of the parent anion is contributed by isomers (C) and (D).

Two neutral structures are exhibited in Figure 4II, in which the global minimum isomer (a) of parent neutral species has a nitric acid ammonia ($HNO_3 \bullet NH_3$) structure, completely different from the crystal structure of ammonium nitrate ($NH_4NO_3$) in bulk solid phase. High energy neutral isomer (b) has the same moiety constituents as those of observed anionic isomers (C) and (D), also containing

hydroxylamine ($NH_2OH$) and nitrous acid (HONO), but with different moiety orientations.

## b) ($NH_4NO_3$ + H) species

Three typical low lying isomers of ($NH_4NO_3$ + H)$^-$ anionic species are shown in Figure 5. The most stable isomer 1H$^-$ (A) contains $NO_2$, $H_2O$, and $NH_3$ moieties, which can be developed from the lowest energy isomer (A) of the parent anion with the $H_2O$ unit formed by adding one H on the OH group. The theoretical VDE of isomer 1H$^-$ (A) is 4.02 eV, much larger than any possible experimental value: it can be eliminated directly. Isomer 1H$^-$ (B) can develop from parent anionic isomer (C) or (D) also containing hydroxylamine ($NH_2OH$). It forms $H_2O$ and NO moieties by adding H on the OH side of nitrous acid (HONO). The structure of isomer 1H$^-$ (B) is completely different from that of isomer 1H$^-$ (A) and the energy difference between isomer 1H$^-$ (B) and 1H$^-$ (A) is 3.28 eV. The VDE of isomer 1H$^-$ (B) is calculated to be 1.60 eV, in good agreement with the experimental determination (1.72 eV). Isomer 1H$^-$ (C) can also develop from parent anionic isomer (C) or (D) by adding H on the O side of nitrous acid (HONO) to form a $NO_2H_2$ moiety. It has a higher energy than that of isomer 1H$^-$ (B) by 1.06 eV. Its calculated VDE (1.71 eV) is also in agreement with the experiments. Therefore, the photoelectron spectrum of ($NH_4NO_3$ + H)$^-$ anionic species is mainly contributed by isomer 1H$^-$ (B). Isomer 1H$^-$ (C) can also exist in the experimental system to contribute to the broad PES feature.

As shown in Figure 6I, three distinct neutral low lying isomers show the same moiety constituents as do the corresponding anionic isomers (Figure 5) but with different spatial arrangements, in which the isomer with an ammonia ($NH_3$) unit is the global minimum structure as well, similar to the situation for the anion.

## c) ($NH_4NO_3$ + 2H) species

The typical low lying isomers of ($NH_4NO_3$ + 2H)$^-$ anionic species are displayed in Figure 7. Isomer 2H$^-$ (A) has a structure consisting of $NH_3$, NO, $H_2O$, and OH moieties. This latter isomer is related to isomer 1H$^-$ (A) through addition of H to the $NO_2$ moiety of 1H$^-$ (A) to form the separate NO and OH components of isomer 2H$^-$ (A). Its calculated VDE is 3.26 eV, higher than the experimental result. Thereby, isomer 2H$^-$ (A) can be excluded from the experimental sample population. Isomers 2H$^-$ (B) to 2H$^-$ (J) all show different structures than that of 2H$^-$ (A) and evidence close energy. They all have geometries with three moieties, including

hydroxylamine ($NH_2OH$), $H_2O$, and nitroxyl (HNO), but with different isomeric conformational characteristics. The theoretical VDE of isomer $2H^-$ (B) is 3.08 eV, larger than possible experimental values. Isomers $2H^-$ (C) to $2H^-$ (J) exhibit calculated VDEs from 2.20 to 2.65 eV, consistent with the experimentally observed range (~2.13 to ~2.63 eV). Therefore, the broad PES feature for ($NH_4NO_3$ + 2H)$^-$ anionic species can be attributed to many coexisting isomers, with hydroxylamine ($NH_2OH$), $H_2O$, and nitroxyl (HNO) characteristics.

Three typical low lying isomers for ($NH_4NO_3$ + 2H) neutral species are displayed in Figure 6II. Higher energy neutral structures evidence configurational similarity to observed anionic isomers, containing hydroxylamine ($NH_2OH$), water ($H_2O$), and nitroxyl (HNO). The most stable neutral isomer 2H (a) has a structure with ammonia ($NH_3$) and water ($H_2O$) units, identical to that of anionic isomer $2H^-$ (A), but with a nitrous acid (HONO) moiety instead of an OH group.

### d) ($NH_4NO_3$ + 3H) species

The low lying isomers of ($NH_4NO_3$ + 3H)$^-$ anionic species are exhibited in Figure 8. They show three different types of structures: one is the lowest energy isomer $3H^-$ (A) with $NH_3$, $H_2O$, OH, and nitroxyl (HNO) moieties; isomer $3H^-$ (C) has two hydroxylamine ($NH_2OH$) moieties and an OH; the remaining isomers all evidence moieties of hydroxylamine ($NH_2OH$), $H_2O$, and $ONH_2$ but with isomeric differences. The theoretical VDEs of isomers $3H^-$ (A) and $3H^-$ (C) are 3.81 and 4.19 eV, larger than the experimental determination from the 355 nm photon PES spectrum. The calculated VDEs of isomers $3H^-$ (B), $3H^-$ (D) to $3H^-$ (G) are 3.09, 2.89, 2.84, 2.75, and 2.95 eV, respectively, higher than the experimental observation. Isomers $3H^-$ (H) and $3H^-$ (I) display calculated VDEs of 2.25 and 2.19 eV, respectively, in reasonable agreement with the experimental value (~1.88 eV). Thus, isomers $3H^-$ (H) and $3H^-$ (I) mainly coexist in experimental sample to contribute to the experimental PES feature.

Three typical low lying isomers of neutral ($NH_4NO_3$ + 3H) species are shown in Figure 6III. High energy neutral isomers 3H (b) and 3H (c) have the same moiety constituents as the observed corresponding anions. The global minimum neutral isomer 3H (a) also has $NH_3$ and $H_2O$ units, similar to anionic isomer $3H^-$ (A), but with an NO moiety instead of a nitroxyl (HNO) group.

### e) ($NH_4NO_3$ + 4H) species

The low lying isomers of ($NH_4NO_3$ + 4H)$^-$ anionic species are displayed in Figure 9. Isomers $4H^-$ (A), (B), (C), and (D) all show structures with $NH_3$, $H_2O$, and

nitroxyl (HNO) moieties, but with different isomeric arrangements. They can develop from the assigned anionic isomers for the smaller clusters and $NH_3$ starts to form. The theoretical VDEs of isomers of 4H$^-$ (A) and 4H$^-$ (B) are 2.98 and 3.03 eV, respectively, higher than the experimental result (~2.35 eV). The calculated VDEs of isomers 4H$^-$ (C) and 4H$^-$ (D) are 2.71 and 2.68 eV, reasonably close to the experimental VDE (~2.35 eV). Isomer 4H$^-$ (E) has a structure which is similar to the lowest energy anionic isomers of smaller clusters with an OH group. Its calculated VDE (4.14 eV) is significantly larger than the experimental determination from the 355 nm photon spectrum. Isomers 4H$^-$ (F) and 4H$^-$ (G) show a $NH_2$ moiety constituent and high calculated VDEs (5.80 and 5.62 eV, respectively). Thus, the PES feature from 355 nm photon spectrum is mainly contributed by isomers 4H$^-$ (C) and 4H$^-$ (D). Isomers 4H$^-$ (A) and 4H$^-$ (B) may also exit in the experiments.

Three typical isomers of $(NH_4NO_3 + 4H)$ neutral species all show the same moiety constituents, including $NH_3$, $H_2O$, nityoxyl (HNO), as shown in Figure 6IV. These structures are different from those of the smaller clusters, for which the neutral structures are more diverse.

## f) $(NH_4NO_3 + 5H)$ species

The typical low lying isomers of $(NH_4NO_3 + 5H)^-$ anionic species are shown in Figure 10. Isomers 5H$^-$ (A) and (B) have structures similar to the lowest energy ones of the smaller clusters $(NH_4NO_3 + nH)^-$ (n = 2-3) with an identifiable OH group. Their calculated VDEs are 4.38 and 4.25 eV, receptively, much higher than the experimentally observed ones from the 355 nm photon PES spectrum. Isomers 5H$^-$ (C) to (F) show moiety constituents of $NH_3$, $H_2O$, and $ONH_2$. They have nearly degenerate energies and theoretical VDEs of 2.80 to 3.24 eV, which are also larger than the experimentally observed features. Isomers 5H$^-$ (G) and (H) also show structural characteristics with $NH_3$, $H_2O$, and $ONH_2$ moieties, and their calculated VDEs (2.55 and 2.53 eV, respectively) are close to the experimental value. Isomers 5H$^-$ (I) and (J) have higher energies than isomers 5H$^-$ (G) and (H) by ~ 0.6 eV. They also contain $NH_3$ and $H_2O$ moieties, but evidence an hydroxyazanyl (HNOH) instead of $ONH_2$. The calculated VDEs of isomers 5H$^-$ (I) and (J) are 2.37 and 2.31 eV. These values are reasonably consistent with the experimental PES (~1.91 eV) VDE. Therefore, both isomers 5H$^-$ (I) and (J) are assigned to contribute to the experimental PES feature. Isomers 5H$^-$ (G) and (H) may also be present too.

Two types of structures can be found for $(NH_4NO_3 + 5H)$ neutral species, as can be seen from Figure 6V. They have the same two types of moiety constituents $(NH_3 \bullet H_2O \bullet ONH_2$ and $NH_3 \bullet H_2O \bullet HNOH)$ as those of assigned anionic isomers, but with different moiety orientations.

## VI DISCUSSION

By directly laser ablating ($\sim 4$ mJ/pulse) an ammonium nitrate solid sample surface, parent anionic species, as well as their hydrogenated cluster anions with up to 5 hydrogens can be observed in the reflectron TOF mass spectrum. With MALDI/ablation processes, only $(NH_4NO_3 + H)^-$ anionic species can be accessed. Based on the good agreement between experimental and theoretical VDEs, as well as the consistent assignments from different DFT computational functionals, the anionic structures of parent anion and hydrogenated cluster anions $(NH_4NO_3 + nH)^-$ (n = 1-5) are validated and assigned. Neutral structures are also provided by employing the experimentally validated calculation algorithm.

### Parent Species

Parent anionic species exist in a $(NH_2OH \bullet HONO)^-$ structure, but not in the crystal structure $NH_4NO_3^-$, or as the lowest energy isomer structure with three moiety constituents $(NH_3 \bullet NO_2 \bullet OH)^-$.

In order to understand the observed parent anionic species from the view point of electronic structure, a Natural Bond Orbital (NBO) analysis is performed based on a $\omega$B97XD/aug-cc-pvtz level of theory. The molecular orbitals of three anionic parent isomers generated from an NBO analysis, are presented in Figure 11.

The NBO/HSOMOs (highest singly occupied molecular orbital) of isomers (A) and (C) display valence bound extra electronic distributions mainly employing a p orbital of O. The NBO/HSOMO of the crystal structure anion (B) shows a diffuse dipole-bound orbital around H atoms of $NH_4$. The electron affinity of isomer (B) is calculated to be -0.02 eV; it is obviously unstable in the anionic form, which may fragment and/or isomerize to a different structure and subsequently transfer its excess electron into a valence orbital. This is probably why an anionic crystal structure form for ammonium nitrate $(NH_4NO_3^-)$ is not found in gas phase. Observation of a fragmentation ion, $NO_3^-$, also illustrates that the crystal structure form for $NH_4NO_3^-$ is not stable in isolation.

Relaxed potential energy surface scans of anionic isomers (A) and (C) along one geometrical coordinate leading to the departure of species with the two N atoms have also been calculated, as shown in Figures 12 and 13. These scans show that the lowest energy isomer (A) will undergo a small energy barrier ($\sim$0.3 eV) to this fragmentation; however, the observed isomer (C) must surmount a significantly larger barrier ($\sim$0.9) to dissociate along this coordinate. This barrier difference is consistent with observation of anionic isomer (C) ($NH_2OH \bullet HONO)^-$ but not isomer (A) ($NH_3 \bullet NO_2 \bullet OH)^-$, which can readily fragment in the ablation source. The observation of fragmentation anions, $NO_2^-$ and $OH^-$, further supports the dissociation reaction of this lowest energy isomer.

The isolated, gas phase neutral structure has a global minimum for $NH_4NO_3$ as ($HNO_3 \bullet NH_3$), different from the solid phase structure of crystalline $NH_4NO_3$. This structural difference can be associated with the long range interactions present for the crystal lattice. Note that for the thermal sublimation/vaporization of the crystal, products ($NH_3 + HNO_3$) are identified.[18]

**Hydrogenated Cluster Species**

Observed isomers for ($NH_4NO_3 + nH)^-$ (n = 1-3) hydrogenated cluster anions share one moiety constituent, hydroxylamine ($NH_2OH$), with the observed parent anion. Starting from n = 4, the $NH_3$ moiety starts to form. The hydrogenation process generates stable/metastable moieties in the cluster anions, including water ($H_2O$), nitroxyl (HNO), ammonia ($NH_3$), or hydroxyazanyl (HNOH) through addition of H atoms. Some intermediates are also formed, for instance, $NO_2H_2$ and $ONH_2$.

The most stable isomers of hydrogenated cluster anions ($NH_4NO_3 + nH)^-$ (n = 1-3, 5), as well as one low energy isomer 4H$^-$ (E) of ($NH_4NO_3 + 4H)^-$, have different moiety constituents than those of the experimentally observed ones at the corresponding same size. The unobserved most stable isomers mainly contain $NH_3$, $H_2O$, and/or OH moieties, while the observed isomers do not form $NH_3$ at n = 1-3 and do not form OH at n = 1-5. The low energy isomers for these series are probably not observed because the parent anionic isomer (A) ($NH_3 \bullet NO_2 \bullet OH)^-$ is absent, and thus its derivative hydrogenated cluster anions are therefore less likely to be formed.

The binding energies of observed isomers 2H$^-$ (C), 3H$^-$ (H), 4H$^-$ (D), and 5H$^-$ (J), and the most stable/low energy isomers 2H$^-$ (A), 3H$^-$ (A), 4H$^-$ (E), and 5H$^-$ (A) for ($NH_4NO_3 + nH)^-$ (n = 2-5) have been given, as shown in the Table S3 of supplementary material. They show that all the binding energies of not observed

isomers are smaller than those of observed isomers by at least ~ 0. 3 eV. They can probably fragment in the ablation source and are not readily formed, and they are not observed in the experiments.

The observed hydrogenated cluster species evolve from observed anionic species $(NH_2OH \bullet HONO)^-$, as they originally share one moiety constituent, hydroxylamine $(NH_2OH)$. The observed hydrogenated cluster species can be formed through parent anion species interacting with an H atom. The H atom can come from primary and secondary dissociated fragments of $NH_4NO_3$, and/or from ubiquitous water in the surroundings.

In order to understand the observed PES VDE trend from the point of view of electronic structure, an NBO analysis of molecular orbitals and charges on specific local atoms of the anions, based on the $\omega$B97XD/aug-cc-pvtz level of theory, are presented in Figures 11 and S22. The HOMOs of observed parent anion and hydrogenated cluster anions exhibit excess electron distribution in the p atomic orbital of an O or N atom. The charge difference between an anion and its corresponding neutral at the anion geometry for a local atom (O or N) of a specific observed anionic isomer is shown in Figure S22. These charge differences exhibit a similar "Z" like pattern with increasing number of added H atoms as do the experimentally observed VDEs. The more negative charge on the local atom of anions correlates with a lower excess electron binding ability and therefore a lower VDE, and vise verse.

The global minimum structures for $(NH_4NO_3 + nH)$ (n = 1-5) hydrogenated cluster neutrals all contain $NH_3$ and $H_2O$ moieties. With increasing number of H atoms, the $NO_2$ can evolve to form HONO, NO, and HNO moieties. These stable moiety structures, along with intermediate species $ONH_2$, can offer insight into reactive intermediates of solid or gas phase ammonium nitrate reaction/dissociation processes.

Finally, the issue of why the lowest energy structures of the various parent and hydrogenated anion clusters are not detected should be addressed beyond the fact that some of them have dipole bound excess electrons (generally VDEs < 0.5 eV) and lower moiety binding energies. First, anion clusters that form in the ablation processes are highly energetic species and are cool in the expansion. Expansion cooling can trap an anion structure in a local potential well that is not the global minimum. Thus, the clusters that survive $(NH_4NO_3 + nH)^-$ (n = 0-5) depend on a considerable set of kinetic phenomena whose rates are a function of the detailed

complete potential energy surface of the particular anion cluster considered. Second, some systems with either small or large VDEs, are simply out of range for detection employing 532, 355, and 266 nm photons.


VII CONCLUSIONS

Anion photoelectron spectroscopic experiments, supported by density functional theoretical studies, provide insights into electronic and geometric structures of gas phase, isolated ammonium nitrate anionic and neutral isomers. Vertical detachment energies (VDE) of parent anionic species and their hydrogenated cluster anions with up to 5 hydrogens are experimentally determined. Their anionic structures are definitively assigned based on good agreement between experimental VDEs and theoretical VDEs. The comparison between experimental and theoretical results demonstrates that the DFT ωB97XD/aug-cc-pvtz level of theory is both reliable and predictive for the electronic characteristics of ammonium nitrate related molecular properties and unimolecular decomposition reactions.

Through laser ablating directly on ammonium nitrate solid sample surface, the parent anion as well as its hydrogenated cluster anions are observed in our RTOFM spectrum. Parent anionic species exists as $(NH_2OH \bullet HONO)^-$ in the gas phase with the excess electron valence bound. $NH_4NO_3^-$ anion with a crystal structure is not present in these experiments, as its extra electron is dipole bound (electron affinity ~ 0 eV). This suggests that the isomerization occurs for ammonium nitrate upon capturing an extra electron and elucidates the active and reactive nature of the ammonium nitrate anion. The calculated global minimum isolated parent neutral species has $HNO_3 \bullet NH_3$ structure, different from the crystal structure in the bulk phase.

The hydrogenated cluster anions can evolve from the parent $(NH_2OH \bullet HONO)^-$ species because they share similar moiety constituents, which are bound together as a single unit through interactions between non covalently bound species within the cluster and are stable on the experimental timescale ( > ~ 100 μs). Adding the first H (n = 1) to the parent anion generates two structures: one anionic structure shows three moieties, including hydroxylamine, water, and nitric oxide; and the other is characterized by hydroxylamine and $NO_2H_2$. At n = 2, many anionic isomers with nearly degenerate energies coexist and contribute to the broad PES feature. They all show geometries with three moieties, including hydroxylamine, water, and nitroxyl, but with isomeric differences. At n = 3, the anionic structure is

characterized by hydroxylamine, water, and $ONH_2$. As the fourth H is added, an ammonia moiety starts to form, which interacts with water and nitroxyl. At n = 5, the ammonia moiety is bound with two water units and hydroxyazanyl or $ONH_2$. The hydrogenation process generates stable moieties in the cluster anions, including water, nitroxyl, ammonia, or hydroxyazanyl.

Based on the evaluated theoretical algorithm, the calculated global minima of hydrogenated cluster neutrals with up to 5 hydrogens all show structure containing ammonia and water moieties. Nitrogen dioxide, nitrous acid, nitric oxide, and nitroxyl can also be found at different particular hydrogenated cluster sizes n = 1, 2, 3, 4.

Studies of the structural characteristics of hydrogenated cluster anions/neutrals can shed light on reactive intermediates or fragmentation products for the reaction/dissociation mechanisms of ammonium nitrate in gas and solid phases. Ammonium nitrate can form reactive intermediates by reacting with H atoms under low energy electron excitation and capture, in which moieties different from thermodynamic dissociation products will be formed, including $NH_2OH$, $NO_2H_2$, $ONH_2$, and $HNOH$. Also, the moieties HNO, NO, $NH_3$, and $H_2O$, identical to thermal decomposition products, can be accessed as observed anions and the global minima of hydrogenated cluster neutrals. The kinetics and dynamics of the isomerization processes associated with parent anionic species can be studied with ultrafast (~ 50 fs) laser techniques.

SUPPLEMENTARY MATERIAL

See supplementary material for more low lying isomers of $(NH_4NO_3 + nH)^-$ (n = 0-5). The moiety/fragment radical names and calculated binding energies of molecular clusters are also provided in the supplementary material. The 266 nm photon PES spectra of $(NH_4NO_3 + nH)^-$ (n = 0-2) and MALDI/ablation results are present too.

ACKNOWLEDGMENTS

# References

1. J. Yin, A. G. Allen, R. M. Harrison, S. G. Jennings, E. Wright, M. Fitzpatrick, T. Healy, E. Barry, D. Ceburnis and D. McCusker, *Atmospheric Res.*, 2005, **78**, 149.

2. R. H. Busch, R. L. Buschbom, W. C. Cannon, K. E. Lauhala, F. J. Miller, J. A. Graham and L. G. Smith, *Environ. Res.*, 1986, **39**, 237.

3. R. S. Park, S. Lee, S. K. Shin and C. H. Song, *Atmos. Chem. Phys.*, 2014, **14**, 2185.

4. G. L. Petriconi and H. M. Papee, *J. Atmos. Sci.*, 1970, **27**, 164.

5. D. M. Laboureur, Z. Han, B. Z. Harding, A. Pineda, W. C. Pittman, C. Rosas, J. Jiang and M. S. Mannan, *J. Hazard. Mater.*, 2016, **308**, 164.

6. W. Pittman, Z. Han, B. Harding, C. Rosas, J. Jiang, A. Pineda and M. S. Mannan, *J. Hazard. Mater.*, 2014, **280**, 472.

7. V. Babrauskas, *J. Fire Sci.*, 2017, **35**, 396.

8. D. L. Hildenbrand, K. H. Lau and D. Chandra, *J. Phys. Chem. B*, 2010, **114**, 330.

9. W.-M. Chien, D. Chandra, K. H. Lau, D. L. Hildenbrand and A. M. Helmy, *J. Chem. Thermodyn.*, 2010, **42**, 846.

10. K. R. Brower, J. C. Oxley and M. Tewari, *J. Phys. Chem.*, 1989, **93**, 4029.

11. W. A. Rosser, S. H. Inami and H. Wise, *J. Phys. Chem.*, 1963, **67**, 1753.

12. D. G. Patil, S. R. Jain and T. B. Brill, *Propellants Explos. Pyrotech. PEP*, 1992, **17**, 99.

13. T. B. Brill, P. J. Brush and D. G. Patil, *Combust. Flame*, 1993, **92**, 178.

14. J. Park and M. C. Lin, *J. Phys. Chem. A*, 2009, **113**, 13556.

15. Z. Han, S. Sachdeva, M. I. Papadaki and M. S. Mannan, *J. Loss Prev. Process Ind.*, 2015, **35**, 307.

16. M. Yang, X. Chen, Y. Wang, B. Yuan, Y. Niu, Y. Zhang, R. Liao and Z. Zhang, *J. Hazard. Mater.*, 2017, **337**, 10.

17. T. P. Russell and T. B. Brill, *Combust. Flame*, 1989, **76**, 393.

18. S. Vyazovkin, J. S. Clawson and C. A. Wight, *Chem. Mater.*, 2001, **13**, 960.

19. B. J. Wood and H. Wise, *J. Chem. Phys.*, 1955, **23**, 693.

20. S. Cagnina, P. Rotureau, G. Fayet and C. Adamo, *Phys. Chem. Chem. Phys.*, 2013, **15**, 10849.

21. J. I. Zink and W. C. Kaska, *J. Am. Chem. Soc.*, 1973, **95**, 7510.

22. L. Pasternack and J. K. Rice, *J. Phys. Chem.*, 1993, **97**, 12805.

23. S. Sreedhar, S. V. Rao, P. P. Kiran, S. P. Tewari and G. M. Kumar, 2010.

24. S. Sunku, A. K. Myakalwar, M. K. Gundawar, P. K. Paturi, S. P. Tewari and V. R. Soma, *ISRN Optics*, 2012, **2012**, 8.

25. M. Hanif, M. Salik and M. A. Baig, *Plasma Phys. Rep.*, 2013, **39**, 1019.

26. H.-S. Im and E. R. Bernstein, *J. Chem. Phys.*, 2000, **113**, 7911.

27. S. Yin and E. R. Bernstein, *J. Chem. Phys.*, 2016, **145**, 154302.

28. B. Yuan, Z. Yu and E. R. Bernstein, *J. Chem. Phys.*, 2015, **142**, 124315.

29. J.-D. Chai and M. Head-Gordon, *Phys. Chem. Chem. Phys.*, 2008, **10**, 6615.

30. Y. Zhao and D. G. Truhlar, *Theor. Chem. Acc.*, 2008, **120**, 215.

31. Y. Zhao and D. G. Truhlar, *Acc. Chem. Res.*, 2008, **41**, 157.

32. M. J. Frisch, G. W. Trucks, H. B. Schlegel, G. E. Scuseria, M. A. Robb, J. R. Cheeseman, G. Scalmani, V. Barone, B. Mennucci, G. A. Petersson, H. Nakatsuji, M. Caricato, X. Li, H. P. Hratchian, A. F. Izmaylov, J. Bloino, G. Zheng, J. L. Sonnenberg, M. Hada, M. Ehara, K. Toyota, R. Fukuda, J. Hasegawa, M. Ishida, T. Nakajima, Y. Honda, O. Kitao, H. Nakai, T. Vreven, J. A. M. Jr., J. E. Peralta, F. Ogliaro, M. Bearpark, J. J. Heyd, E. Brothers, K. N. Kudin, V. N. Staroverov, R. Kobayashi, J. Normand, K. Raghavachari, A. Rendell, J. C. Burant, S. S. Iyengar, J. Tomasi, M. Cossi, N. Rega, J. M. Millam, M. Klene, J. E. Knox, J. B. Cross, V. Bakken, C. Adamo, J. Jaramillo, R. Gomperts, R. E. Stratmann, O. Yazyev, A. J. Austin, R. Cammi, C. Pomelli, J. W. Ochterski, R. L.

Martin, K. Morokuma, V. G. Zakrzewski, G. A. Voth, P. Salvador, J. J. Dannenberg, S. Dapprich, A. D. Daniels, O. Farkas, J. B. Foresman, J. V. Ortiz, J. Cioslowski and D. J. Fox, *Gaussian 09, Revision A.02, Gaussian, Inc., Wallingford CT*, 2009.

33.     L. A. Burns, Á. V.-. Mayagoitia, B. G. Sumpter and C. D. Sherrill, *J. Chem. Phys.*, 2011, **134**, 084107.

34.     J. Klyne, M. Schmies, M. Miyazaki, M. Fujii and O. Dopfer, *Phys. Chem. Chem. Phys.*, 2018, **20**, 3148.
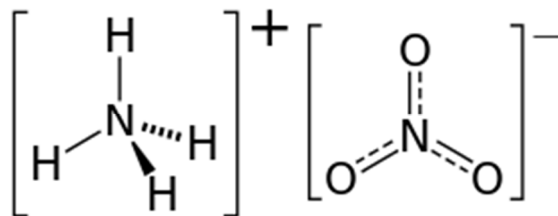
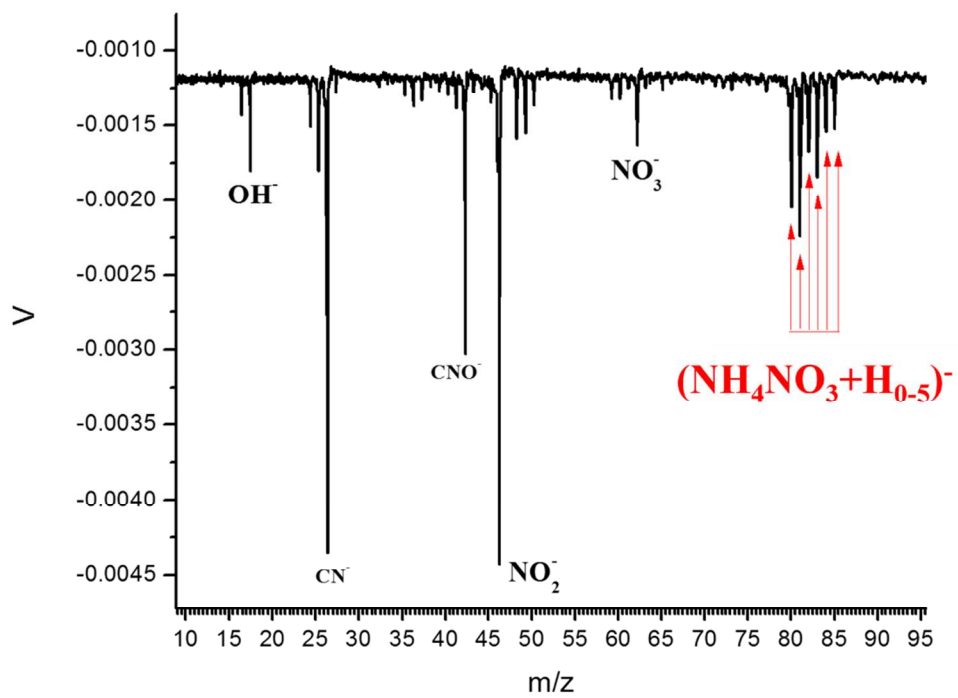Figure 1 Schematic structures of ammonium nitrate (from Wikipedia).
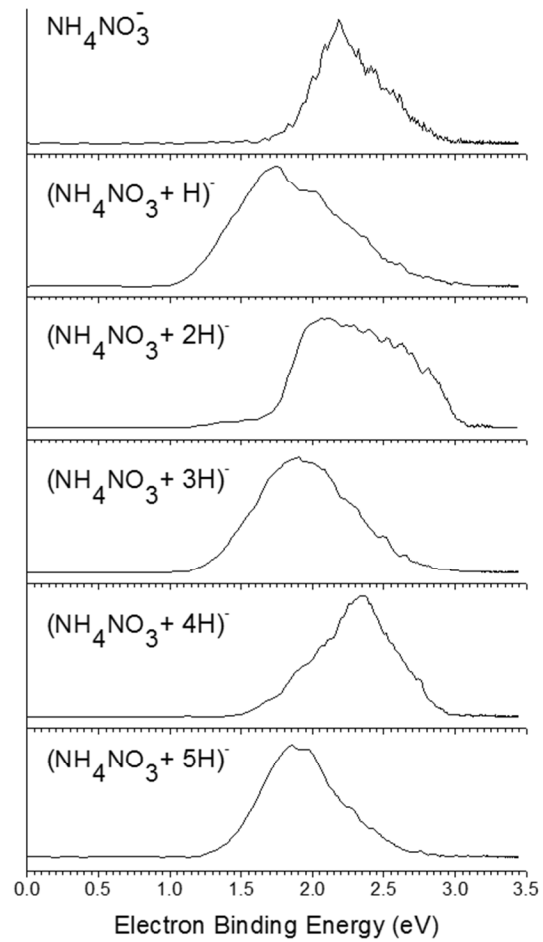


Figure 2 Mass spectrum of $(NH_4NO_3 + nH)^-$.

Figure 3 Photoelectron spectra of $(NH_4NO_3 + nH)^-$ (n = 0-5) recorded with 355 nm photons.

**anions**



**(A) 0.00 eV**
nitrogen dioxide + hydroxyl + ammonia

**(B) 0.69 eV**
ammonium nitrate

I

**(C) 0.79 eV**
hydroxylamine + nitrous acid

**(D) 0.81 eV**
hydroxylamine + nitrous acid

**neutrals**

II

**(a) 0.00 eV**
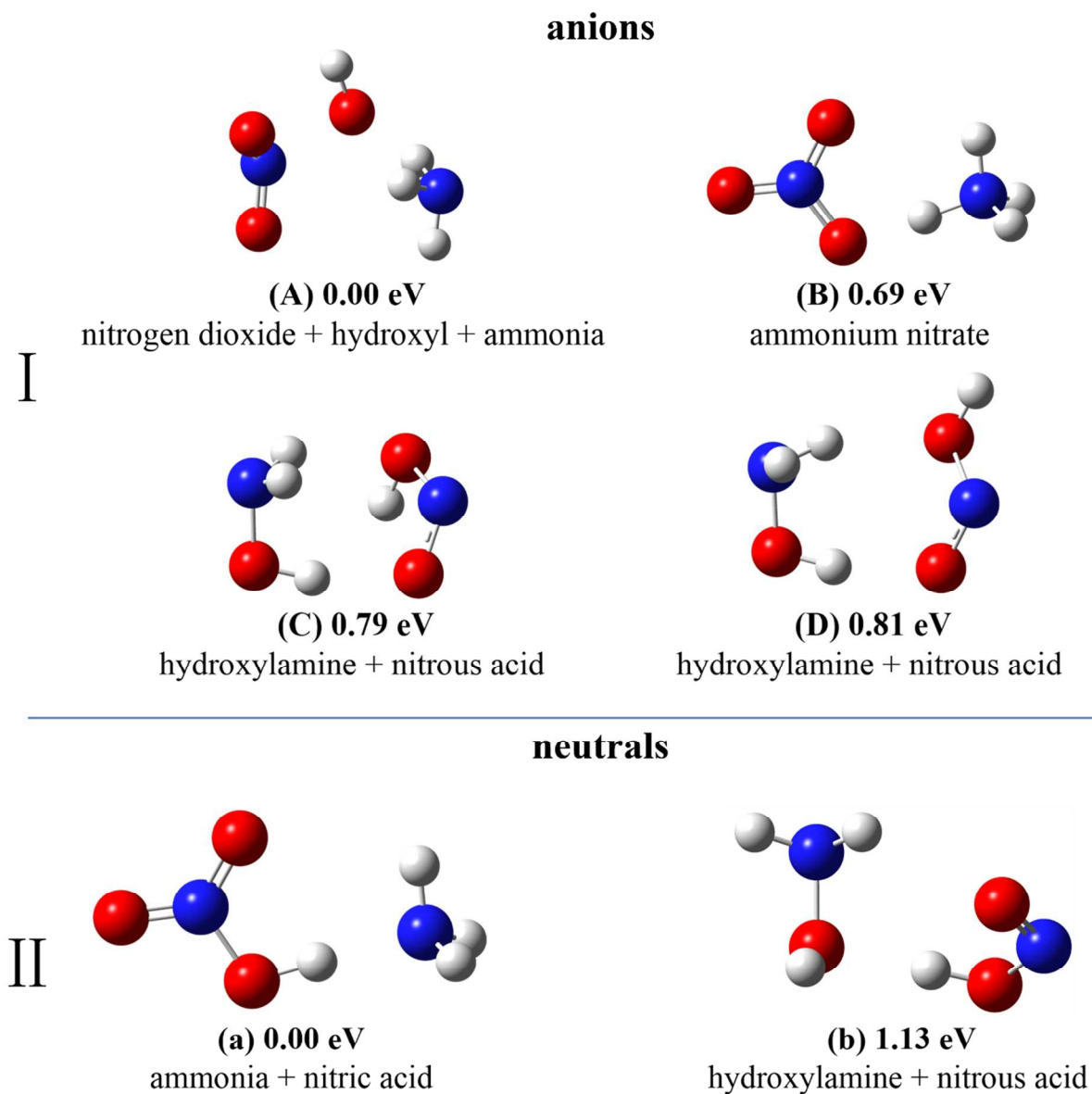ammonia + nitric acid

**(b) 1.13 eV**
hydroxylamine + nitrous acid

Figure 4 (I) Optimized geometries of typical low lying anionic isomers of parent anion based on ωB97XD/aug-cc-pvtz DFT calculations. (II) Optimized geometries of typical low lying neutral isomers of parent neutral based on ωB97XD/aug-cc-pvtz DFT calculations. The relative energies and structural polymorphs are indicated. O red, N blue, H white. (For more information on anions, see Table 1) (VDE of (A): 3.83 eV; VDE of (B): 0.45 eV; VDE of (C): 2.07 eV; VDE of (D): 2.10 eV)
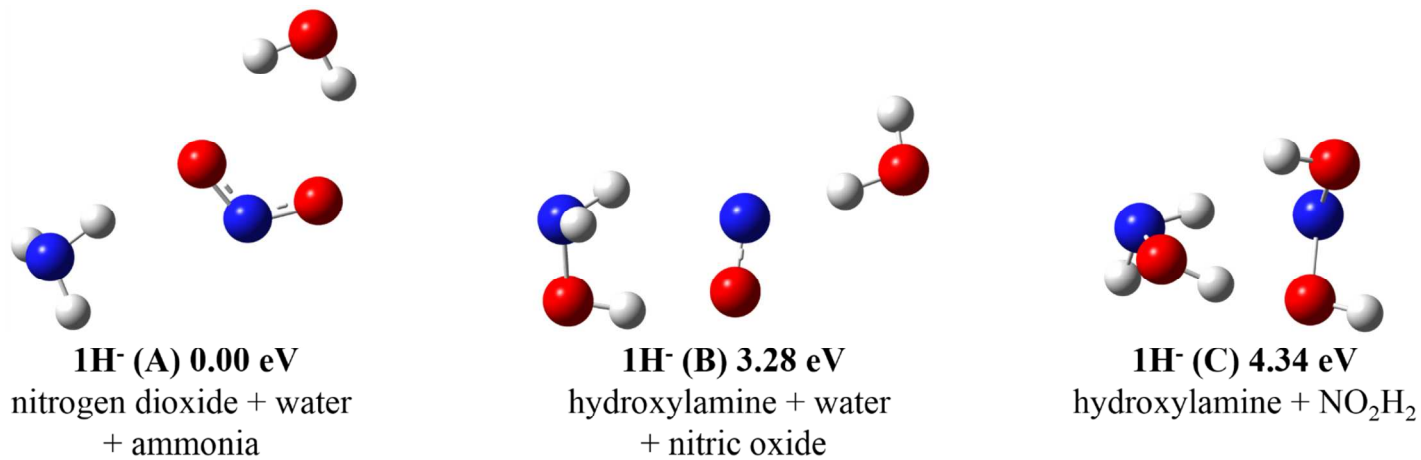
**1H⁻ (A) 0.00 eV**
nitrogen dioxide + water
+ ammonia

**1H⁻ (B) 3.28 eV**
hydroxylamine + water
+ nitric oxide

**1H⁻ (C) 4.34 eV**
hydroxylamine + $NO_2H_2$

Figure 5 Optimized geometries of typical low lying anionic isomers of $(NH_4NO_3+H)^-$ based on ωB97XD/aug-cc-pvtz DFT calculations. The relative energies and structural polymorphs are indicated. (For more information on anions, see Table 1) (VDE of 1H⁻ (A): 4.02 eV; VDE of 1H⁻ (B): 1.60 eV; VDE of 1H⁻ (C): 1.71 eV)
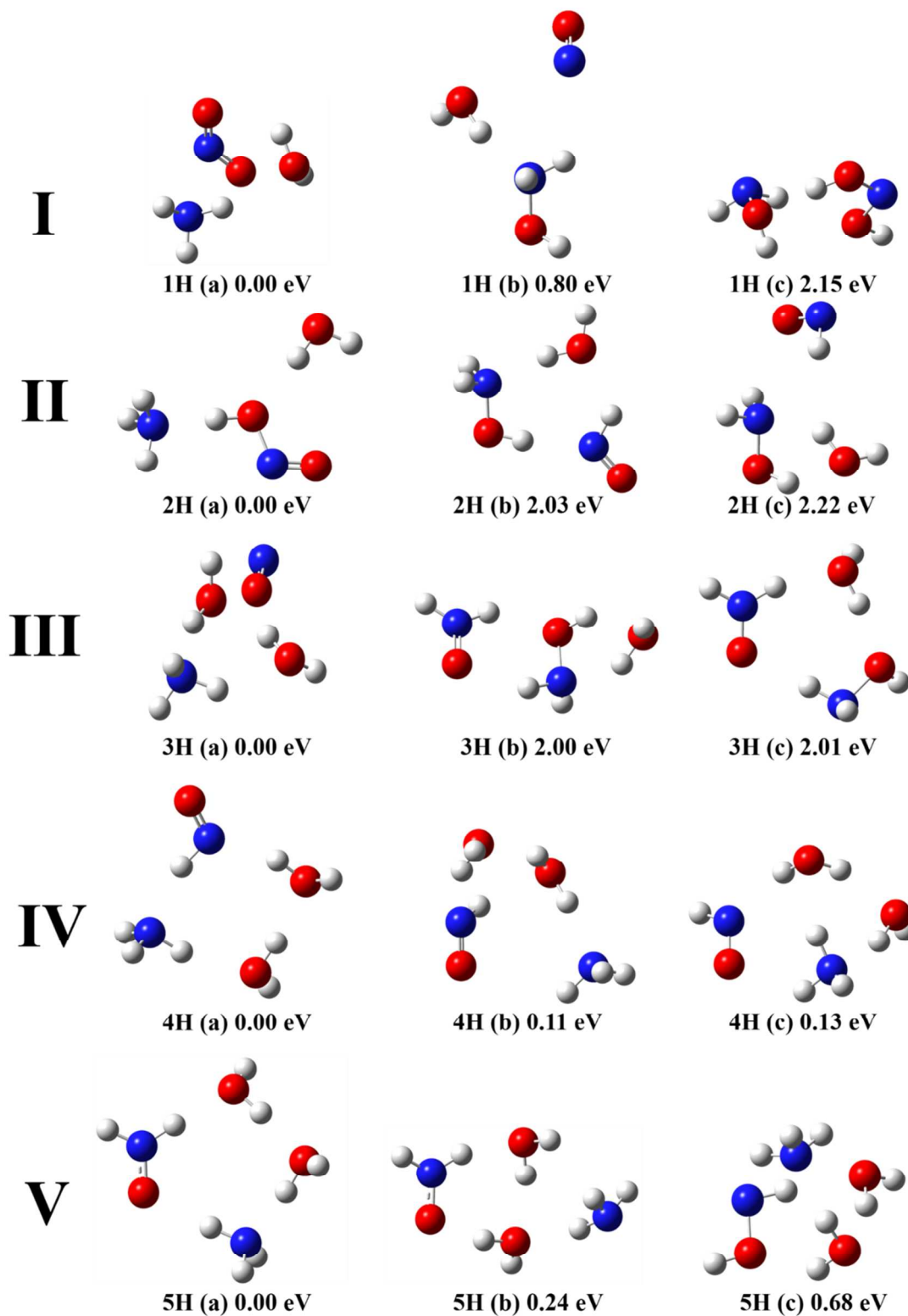
Figure 6 Optimized geometries of typical low lying neutral isomers of (NH₄NO₃+nH) (n = 1-5; I, II, III, IV, and V, respectively) based on ωB97XD/aug-cc-pvtz DFT calculations. The relative energies are indicated.

**2H⁻ (A) 0.00 eV**
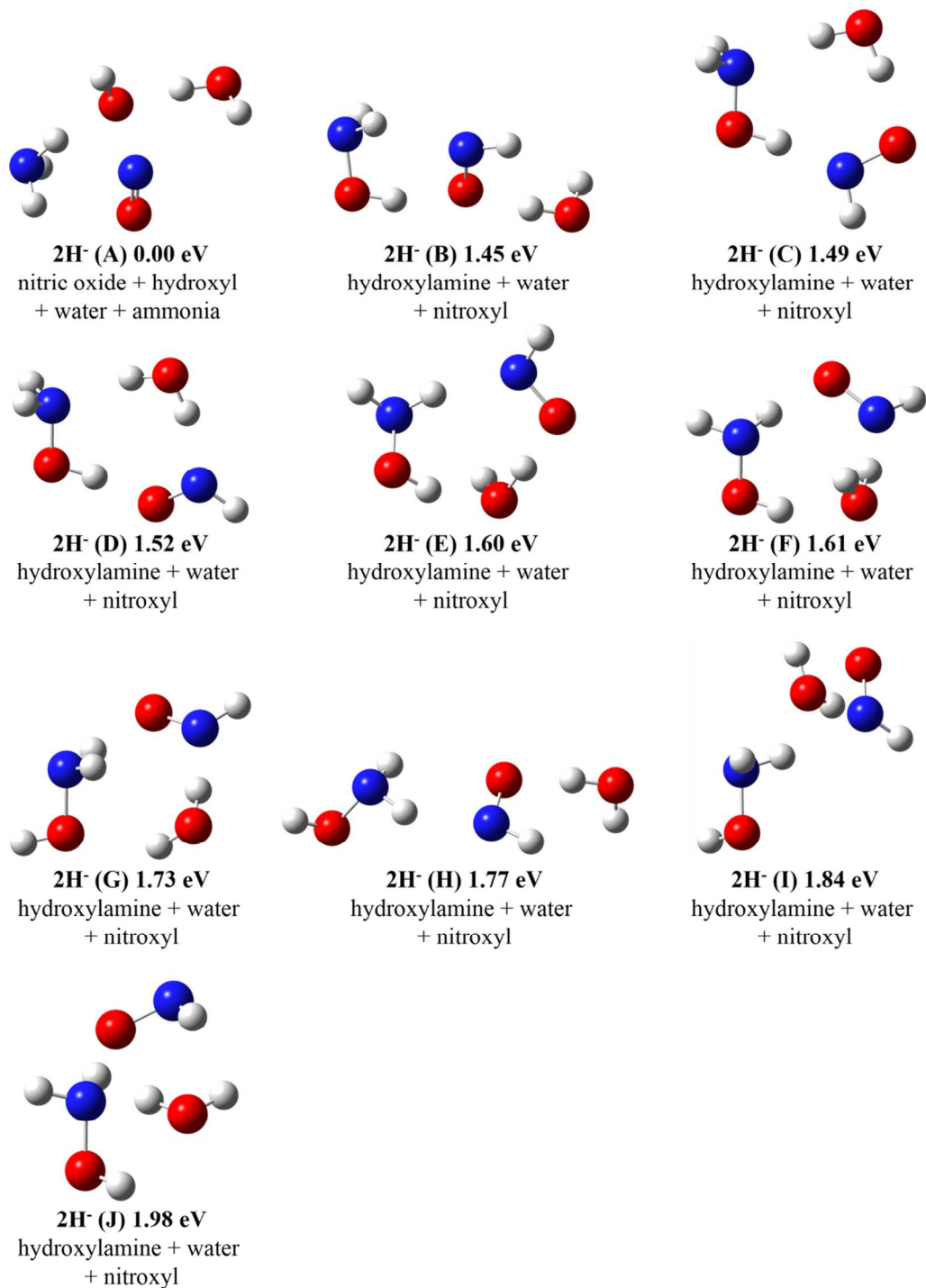nitric oxide + hydroxyl
+ water + ammonia

**2H⁻ (B) 1.45 eV**
hydroxylamine + water
+ nitroxyl

**2H⁻ (C) 1.49 eV**
hydroxylamine + water
+ nitroxyl

**2H⁻ (D) 1.52 eV**
hydroxylamine + water
+ nitroxyl

**2H⁻ (E) 1.60 eV**
hydroxylamine + water
+ nitroxyl

**2H⁻ (F) 1.61 eV**
hydroxylamine + water
+ nitroxyl

**2H⁻ (G) 1.73 eV**
hydroxylamine + water
+ nitroxyl

**2H⁻ (H) 1.77 eV**
hydroxylamine + water
+ nitroxyl

**2H⁻ (I) 1.84 eV**
hydroxylamine + water
+ nitroxyl

**2H⁻ (J) 1.98 eV**
hydroxylamine + water
+ nitroxyl

Figure 7 Optimized geometries of typical low lying anionic isomers of $(NH_4NO_3+2H)^-$ based on ωB97XD/aug-cc-pvtz DFT calculations. The relative energies and structural polymorphs are indicated. (For more information on anions, see Table 1) (VDE of 2H⁻ (A): 3.26 eV; VDE of 2H⁻ (B): 3.08 eV; VDE of 2H⁻ (C): 2.52 eV; VDE of 2H⁻ (D): 2.55 eV; VDE of 2H⁻ (E): 2.65 eV; VDE of 2H⁻ (F): 2.55 eV; VDE of 2H⁻ (G): 2.35 eV; VDE of 2H⁻ (H): 2.50 eV; VDE of 2H⁻ (I): 2.27 eV; VDE of 2H⁻ (J): 2.20 eV)
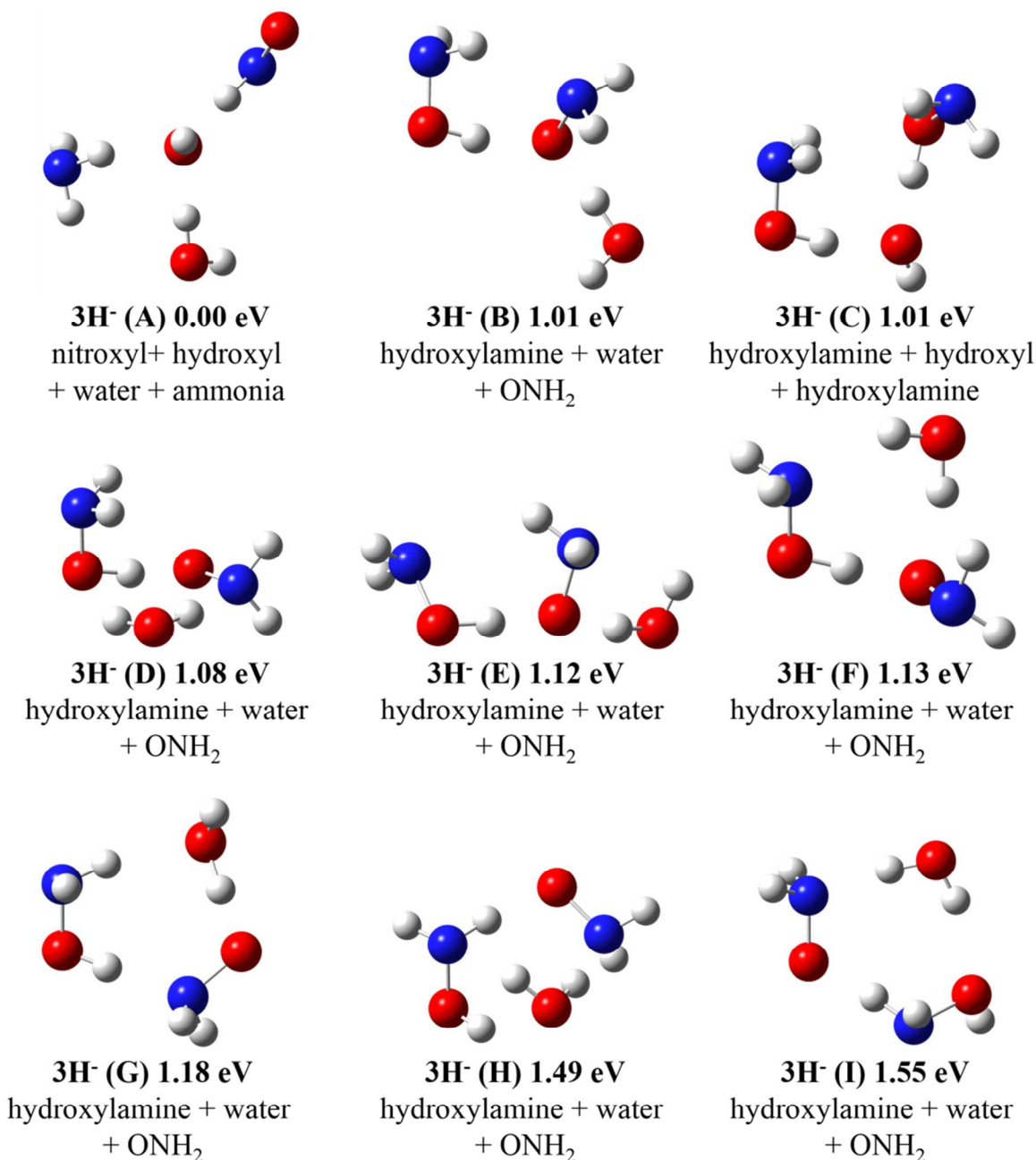
**3H⁻ (A) 0.00 eV**
nitroxyl+ hydroxyl
+ water + ammonia

**3H⁻ (B) 1.01 eV**
hydroxylamine + water
+ ONH₂

**3H⁻ (C) 1.01 eV**
hydroxylamine + hydroxyl
+ hydroxylamine

**3H⁻ (D) 1.08 eV**
hydroxylamine + water
+ ONH₂

**3H⁻ (E) 1.12 eV**
hydroxylamine + water
+ ONH₂

**3H⁻ (F) 1.13 eV**
hydroxylamine + water
+ ONH₂

**3H⁻ (G) 1.18 eV**
hydroxylamine + water
+ ONH₂

**3H⁻ (H) 1.49 eV**
hydroxylamine + water
+ ONH₂

**3H⁻ (I) 1.55 eV**
hydroxylamine + water
+ ONH₂

Figure 8 Optimized geometries of typical low lying anionic isomers of $(NH_4NO_3+3H)^-$ based on ωB97XD/aug-cc-pvtz DFT calculations. The relative energies and structural polymorphs are indicated. (For more information on anions, see Table 1) (VDE of 3H⁻ (A): 3.81 eV; VDE of 3H⁻ (B): 3.09 eV; VDE of 3H⁻ (C): 4.19 eV; VDE of 3H⁻ (D): 2.89 eV; VDE of 3H⁻ (E): 2.84 eV; VDE of 3H⁻ (F): 2.75 eV; VDE of 3H⁻ (G): 2.95 eV; VDE of 3H⁻ (H): 2.25 eV; VDE of 3H⁻ (I): 2.19 eV)
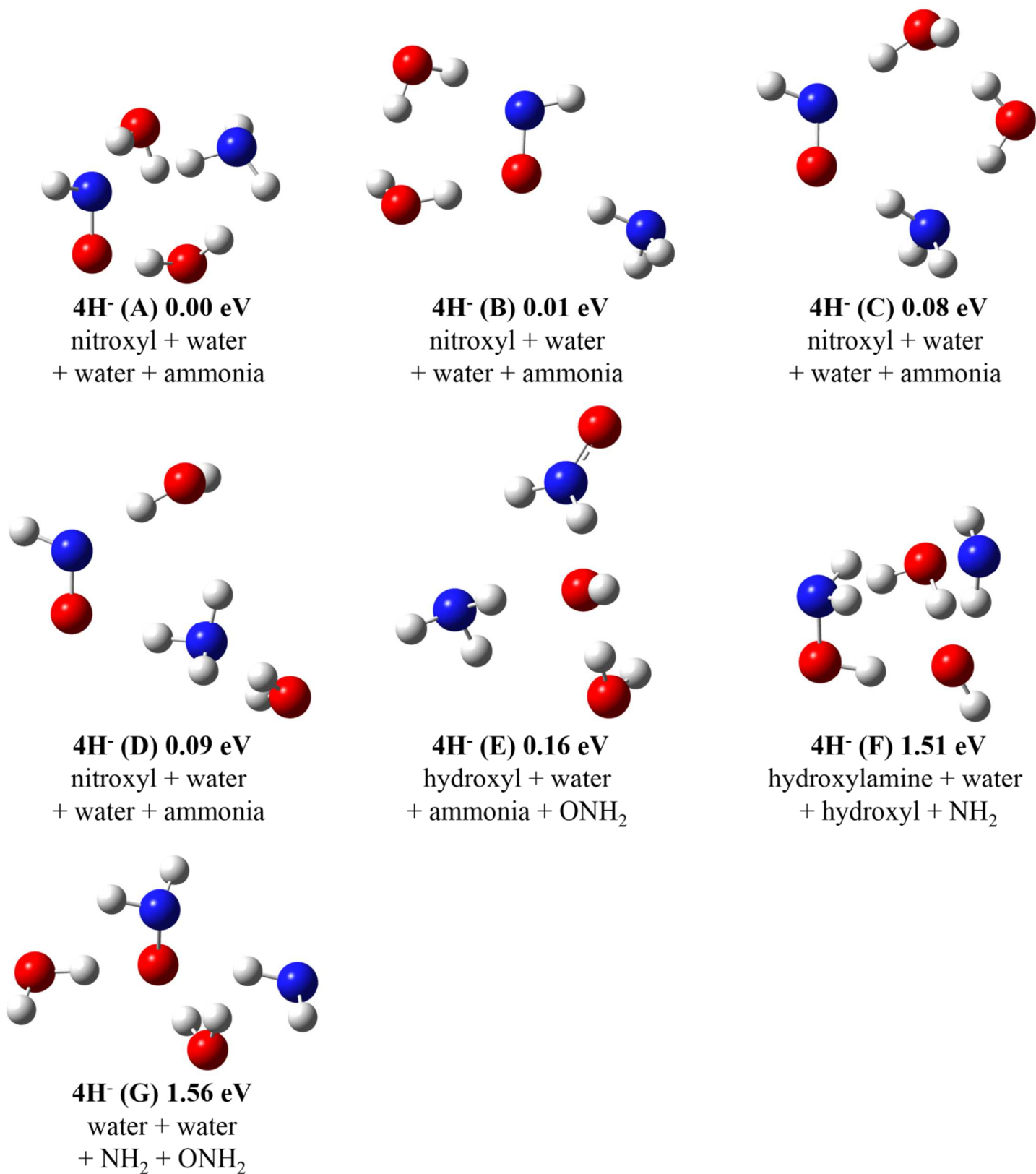
**4H⁻ (A) 0.00 eV**
nitroxyl + water
+ water + ammonia

**4H⁻ (B) 0.01 eV**
nitroxyl + water
+ water + ammonia

**4H⁻ (C) 0.08 eV**
nitroxyl + water
+ water + ammonia

**4H⁻ (D) 0.09 eV**
nitroxyl + water
+ water + ammonia

**4H⁻ (E) 0.16 eV**
hydroxyl + water
+ ammonia + $ONH_2$

**4H⁻ (F) 1.51 eV**
hydroxylamine + water
+ hydroxyl + $NH_2$

**4H⁻ (G) 1.56 eV**
water + water
+ $NH_2$ + $ONH_2$

Figure 9 Optimized geometries of typical low lying anionic isomers of $(NH_4NO_3+4H)^-$ based on ωB97XD/aug-cc-pvtz DFT calculations. The relative energies and structural polymorphs are indicated. (For more information on anions, see Table 1) (VDE of 4H⁻ (A): 2.98 eV; VDE of 4H⁻ (B): 3.03 eV; VDE of 4H⁻ (C): 2.71 eV; VDE of 4H⁻ (D): 2.68 eV; VDE of 4H⁻ (E): 4.14 eV; VDE of 4H⁻ (F): 5.80 eV; VDE of 4H⁻ (G): 5.62 eV)
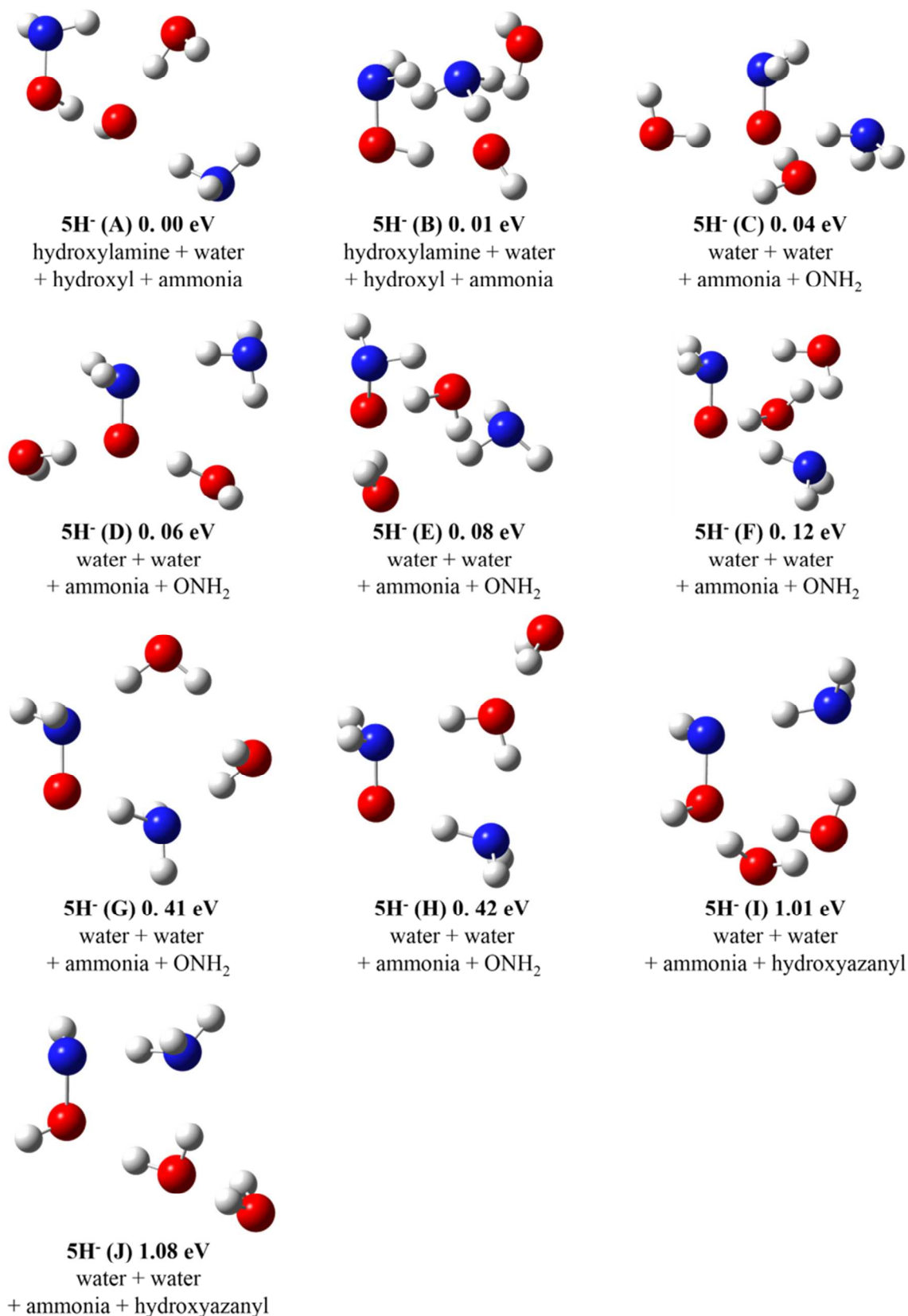
**5H⁻ (A) 0. 00 eV**
hydroxylamine + water
+ hydroxyl + ammonia

**5H⁻ (B) 0. 01 eV**
hydroxylamine + water
+ hydroxyl + ammonia

**5H⁻ (C) 0. 04 eV**
water + water
+ ammonia + ONH$_2$

**5H⁻ (D) 0. 06 eV**
water + water
+ ammonia + ONH$_2$

**5H⁻ (E) 0. 08 eV**
water + water
+ ammonia + ONH$_2$

**5H⁻ (F) 0. 12 eV**
water + water
+ ammonia + ONH$_2$

**5H⁻ (G) 0. 41 eV**
water + water
+ ammonia + ONH$_2$

**5H⁻ (H) 0. 42 eV**
water + water
+ ammonia + ONH$_2$

**5H⁻ (I) 1.01 eV**
water + water
+ ammonia + hydroxyazanyl

**5H⁻ (J) 1.08 eV**
water + water
+ ammonia + hydroxyazanyl

Figure 10 Optimized geometries of typical low lying anionic isomers of (NH$_4$NO$_3$+5H)⁻ based on ωB97XD/aug-cc-pvtz DFT calculations. The relative energies and structural polymorphs are indicated. (For more information on anions, see Table 1) (VDE of 5H⁻ (A): 4.38 eV; VDE of 5H⁻ (B): 4.25 eV; VDE of 5H⁻ (C): 3.24 eV; VDE of 5H⁻ (D): 3.23 eV; VDE of 5H⁻ (E): 3.15 eV; VDE of 5H⁻ (F): 2.80 eV; VDE of 5H⁻ (G): 2.55 eV; VDE of 5H⁻ (H): 2.53 eV; VDE of 5H⁻ (I): 2.37 eV; VDE of 5H⁻ (J): 2.31 eV)
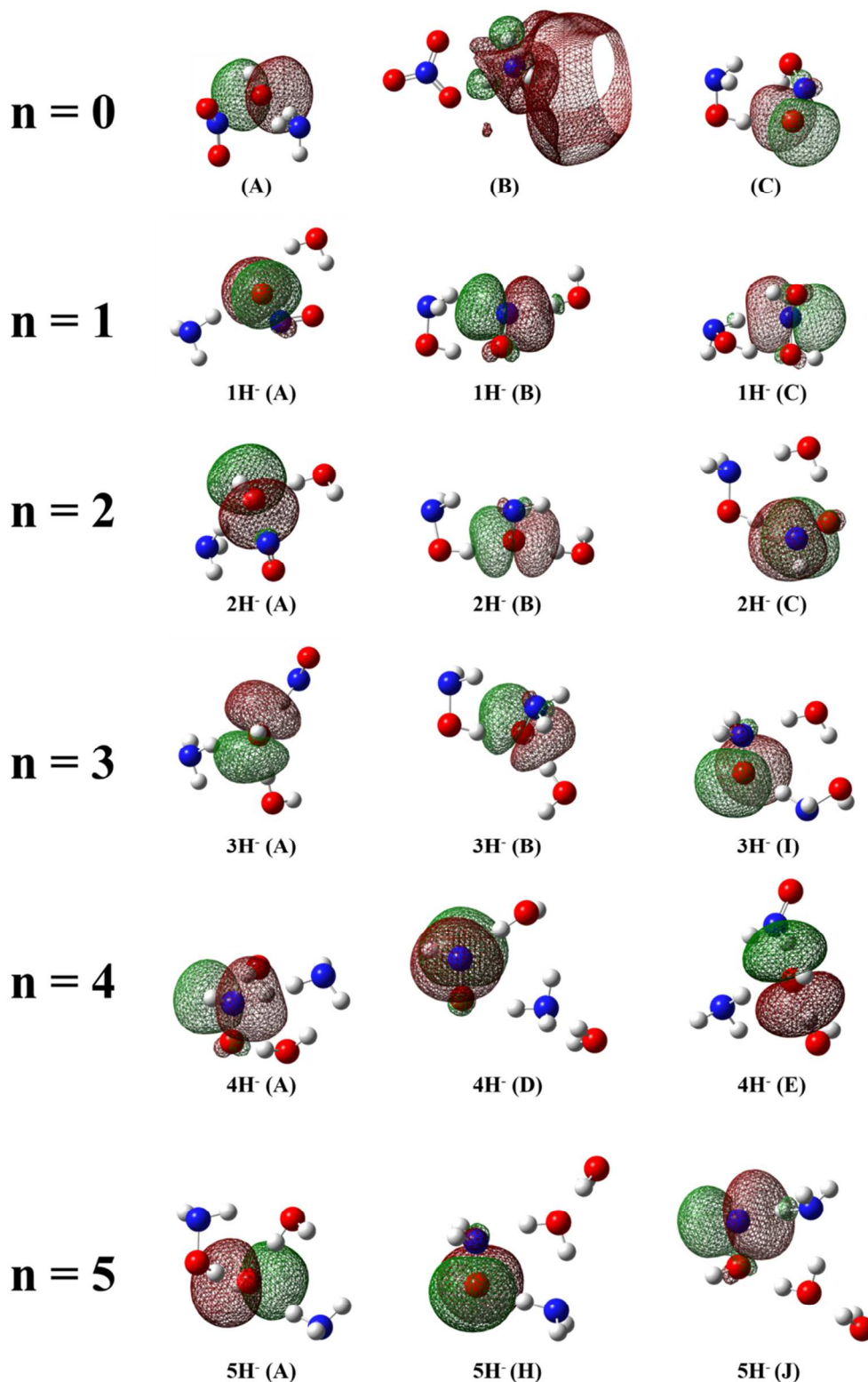
Figure 11 NBO/HOMOs (highest occupied molecular orbitals) of several typical low lying isomers of $(NH_4NO_3 + nH)^-$ (n = 0-5) anions from an NBO analysis based on ωB97XD/aug-cc-pvtz DFT calculations. Ammonium nitrite parent anion (B) mostly displays dipole bound character with the added electron distributing around H atoms of ammonium unit, while the remaining isomers all show valence bound extra electron wave functions mostly localized on O/N p orbitals.
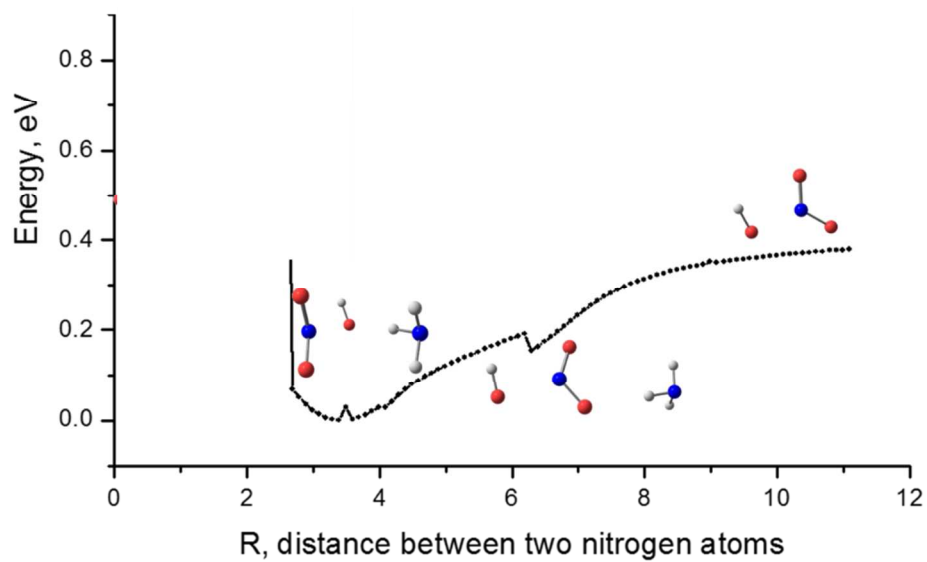
Figure 12. Relaxed Potential Energy Surface scan of ammonium nitrate anionic isomer (A) $(NH_3 \bullet OH \bullet NO_2)^-$ through separation into two moieties. R(Å): distance between two nitrogen atoms.
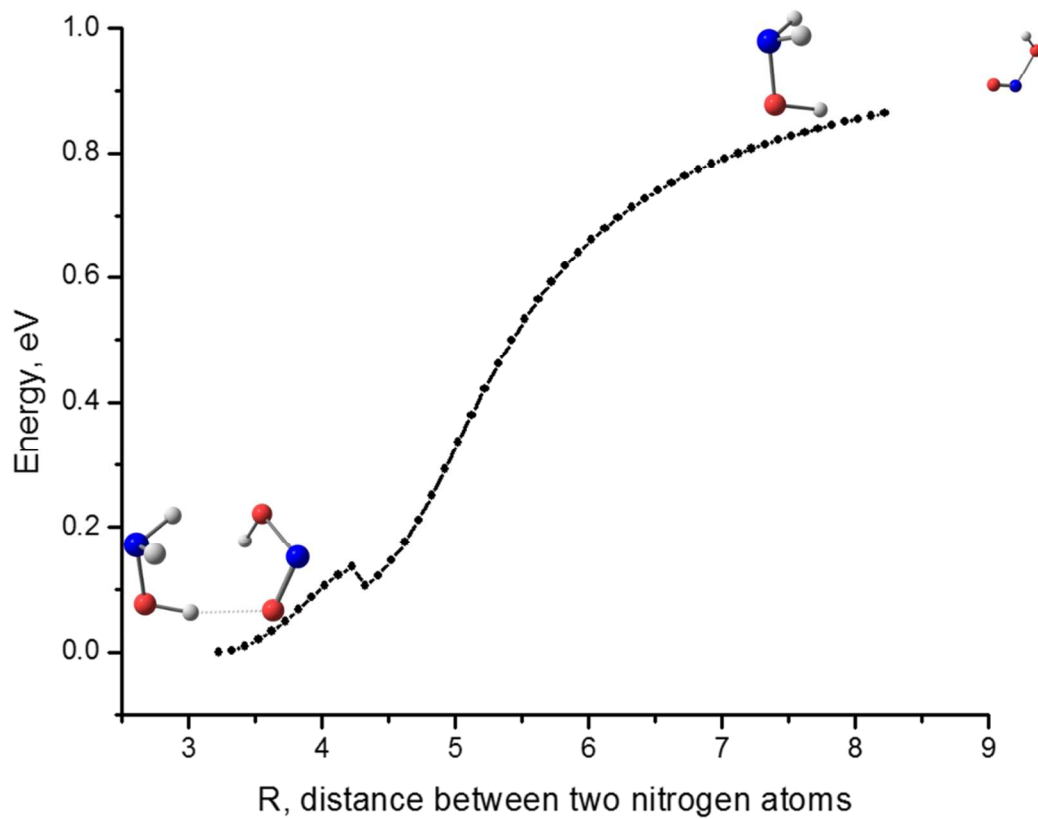
Figure 13. Relaxed Potential Energy Surface scan of ammonium nitrate anionic isomer (C) $(NH_2OH \bullet HONO)^-$ through separation into two moieties. $R(\text{Å})$: distance between two nitrogen atoms.

Table 1 Relative energies (ΔE) of the low energy isomers of $(NH_4NO_3 + nH)^-$ (n = 0-5), and comparison of their calculated VDEs based on ωB97XD/aug-cc-pvtz and M062X/aug-cc-pvtz DFT algorithms. Experimental VDE values are given in the right hand column. All energies are in eV. The labels in bold indicate the isomers which are assigned to contribute most prominently to the experimental spectra features.

| | | M062X/aug-cc-pvtz | | ωB97XD/aug-cc-pvtz | | Exp. VDE |
|---|---|---|---|---|---|---|
| | | ΔE | Theo. VDE | ΔE | Theo. VDE | |
| $NH_4NO_3^-$ | (A) | 0.00 | 3.87 | 0.00 | 3.83 | |
| | (B) | 0.62 | 0.43 | 0.69 | 0.45 | |
| | **(C)** | 0.53 | 2.18 | 0.79 | 2.07 | ~2.18 |
| | **(D)** | 0.59 | 2.12 | 0.81 | 2.10 | |
| | | | | | | |
| $(NH_4NO_3 + H)^-$ | 1H⁻ (A) | 0.00 | 4.28 | 0.00 | 4.02 | |
| | **1H⁻ (B)** | 3.17 | 1.79 | 3.28 | 1.60 | ~1.72 |
| | 1H⁻ (C) | 4.14 | 1.85 | 4.34 | 1.71 | |
| | | | | | | |
| $(NH_4NO_3 + 2H)^-$ | 2H⁻ (A) | 0.00 | 3.68 | 0.00 | 3.26 | |
| | 2H⁻ (B) | 1.35 | 3.21 | 1.45 | 3.08 | |
| | **2H⁻ (C)** | 1.42 | 2.68 | 1.49 | 2.52 | ~2.13 to ~2.63 |
| | **2H⁻ (D)** | 1.45 | 2.74 | 1.52 | 2.55 | |
| | **2H⁻ (E)** | 1.51 | 2.77 | 1.60 | 2.65 | |
| | **2H⁻ (F)** | 1.53 | 2.61 | 1.61 | 2.55 | |
| | **2H⁻ (G)** | 1.66 | 2.43 | 1.73 | 2.35 | |
| | **2H⁻ (H)** | 1.69 | 2.64 | 1.77 | 2.50 | |
| | **2H⁻ (I)** | 1.67 | 2.48 | 1.84 | 2.27 | |
| | **2H⁻ (J)** | 1.53 | 2.61 | 1.98 | 2.20 | |
| | | | | | | |
| $(NH_4NO_3 + 3H)^-$ | 3H⁻ (A) | 0.00 | 4.03 | 0.00 | 3.81 | |
| | 3H⁻ (B) | 0.89 | 3.44 | 1.01 | 3.09 | |
| | 3H⁻ (C) | 0.88 | 4.51 | 1.01 | 4.19 | |
| | 3H⁻ (D) | 0.93 | 3.20 | 1.08 | 2.89 | |
| | 3H⁻ (E) | 0.98 | 3.20 | 1.12 | 2.84 | |
| | 3H⁻ (F) | 0.99 | 3.23 | 1.13 | 2.75 | |
| | 3H⁻ (G) | 1.09 | 3.33 | 1.18 | 2.95 | |
| | **3H⁻ (H)** | 1.40 | 2.52 | 1.49 | 2.25 | |
| | **3H⁻ (I)** | 1.49 | 2.44 | 1.55 | 2.19 | ~1.88 |
| | | | | | | |
| $(NH_4NO_3 + 4H)^-$ | 4H⁻ (A) | 0.00 | 3.10 | 0.00 | 2.98 | |
| | 4H⁻ (B) | 0.03 | 3.14 | 0.01 | 3.03 | |
| | **4H⁻ (C)** | 0.13 | 2.82 | 0.08 | 2.71 | |
| | **4H⁻ (D)** | 0.15 | 2.78 | 0.09 | 2.68 | ~2.35 |
| | 4H⁻ (E) | 0.21 | 4.22 | 0.16 | 4.14 | |
| | 4H⁻ (F) | 1.43 | 6.16 | 1.51 | 5.80 | |
| | 4H⁻ (G) | 1.50 | 6.01 | 1.56 | 5.62 | |
| | | | | | | |
| $(NH_4NO_3 + 5H)^-$ | 5H⁻ (A) | 0.03 | 3.31 | 0.00 | 4.38 | |
| | 5H⁻ (B) | 0.00 | 4.48 | 0.01 | 4.25 | |
| | 5H⁻ (C) | 0.04 | 3.57 | 0.04 | 3.24 | |
| | 5H⁻ (D) | 0.08 | 3.20 | 0.06 | 3.23 | |
| | 5H⁻ (E) | 0.05 | 3.46 | 0.08 | 3.15 | |
| | 5H⁻ (F) | 0.11 | 3.06 | 0.12 | 2.80 | |
| | **5H⁻ (G)** | 0.43 | 2.74 | 0.41 | 2.55 | |
| | **5H⁻ (H)** | 0.44 | 2.73 | 0.42 | 2.53 | |
| | **5H⁻ (I)** | 1.00 | 2.52 | 1.01 | 2.37 | |
| | **5H⁻ (J)** | 1.08 | 2.44 | 1.08 | 2.31 | ~1.91 |

Parent anionic species exists as $(NH_2OH\bullet HONO)^-$ with the extra electron valence bound. The hydrogenated cluster anions can evolve from $(NH_2OH\bullet HONO)^-$.